NASA Technical Memorandum 81358

COMPARISON OF THEORETICAL PREDICTIONS OF ORBITER AIRLOADS WITH WIND TUNNEL AND FLIGHT TEST RESULTS FOR A MACH NUMBER OF 0.52

Alan L. Carter and Robert L. Sims

May 1981

NASA

NASA Technical Memorandum 81358

COMPARISON OF THEORETICAL PREDICTIONS OF ORBITER AIRLOADS WITH WIND TUNNEL AND FLIGHT TEST RESULTS FOR A MACH NUMBER OF 0.52

Alan L. Carter and Robert L. Sims
Dryden Flight Research Center
Edwards, California

National Aeronautics and
Space Administration

1981

COMPARISON OF THEORETICAL PREDICTIONS OF ORBITER AIRLOADS WITH WIND TUNNEL AND FLIGHT TEST RESULTS FOR A MACH NUMBER OF 0.52

Alan L. Carter and Robert L. Sims
Dryden Flight Research Center

INTRODUCTION

The better we are able to predict airloads, the more efficient the airframes we are able to design. Our ability to predict airloads is improved through the analysis of flight measurements and wind tunnel tests, and through the development of theoretical analysis.

The air vehicle development process has several phases: (1) the analytical investigation of a large number of candidate configurations in the preliminary design phase; (2) wind tunnel tests to fine-tune the configuration and to establish its rigid aerodynamic characteristics; (3) analytical predictions of the effects of flexibility; (4) design, fabrication, and ground test of the prototype vehicle; and (5) flight test, which is the final proof of the concept.

Currently, large computer-aided design systems are being developed with the objective of automating as much of the development cycle as possible. These systems are completely dependent on the accuracy of the analytical methods used. Realistic evaluation of the accuracy of these methods is obtained from comparison with experimental results, especially flight test.

Since the instrumentation, calibration, and flight testing of full scale air vehicles are expensive, most aeronautical research is conducted through wind tunnel testing and computer analysis. It is, however, necessary to obtain flight measurements from time to time to evaluate these prediction techniques.

Presented herein are flight test results for the space shuttle orbiter (OV-101) wing loads measured during the approach and landing test (ALT) program conducted at the NASA Dryden Flight Research Center (DFRC) at Edwards, Calif. during 1977. The flight test results are compared with both wind tunnel predictions and the predictions from a FLEXSTAB analysis computer model. From these comparisons, an assessment is made

regarding the current capability for airload measurement and prediction on a low aspect ratio double delta aerodynamic configuration.

Recognition is due to Rodney Rocha, of the NASA Johnson Space Center (JSC), for supplying flight and wind tunnel data; Donald Black, DFRC, for programming support; Kenneth Iliff, DFRC, for supplying basic aircraft parameters; and to the Air Force Flight Test Center (AFFTC) for the ground tracking data.

SYMBOLS AND ABBREVIATIONS

a_{b_i}, a_{t_i}, a_{v_i}	load equation coefficients
B_A	wing airload bending, N-m (in-lb)
B_N	wing net bending, N-m (in-lb)
b	vehicle reference span, m (in.)
b_w	wing reference span, m (in.)
C_B	wing bending load parameter, $\frac{B_A}{\bar{q}}$
C_L	lift coefficient, $\frac{L}{\bar{q}S}$
C_M	pitching moment coefficient, $\frac{M}{\bar{q}S\bar{c}}$
C_T	wing torque load parameter, $\frac{T_A}{\bar{q}}$
C_V	wing shear load parameter, $\frac{V_A}{\bar{q}}$
$\bar{c}$	vehicle reference chord, m (in.)
$\bar{c}_w$	wing reference chord, m (in.)
F.S.	fuselage station
g	acceleration due to gravity, m/sec^2 (ft/sec^2)

HM_{ib}	hinge moment of inboard elevon, N-m (in-lb)
HM_{ob}	hinge moment of outboard elevon, N-m (in-lb)
h	altitude, m (ft)
I_{XX}, I_{XZ}, I_{YY}, I_{ZZ}	components of moment of inertia about body axes, $kg\text{-}m^2$ ($slug\text{-}ft^2$)
L	total lift, N (lb)
L_B	vehicle body length
M	total pitching moment, N-m (in-lb)
N_y	lateral load factor, g
N_z	normal load factor, g
$\bar{q}$	dynamic pressure, N/m^2 (psf)
$\dot{q}_c$	computed pitch acceleration, deg/sec^2
S	vehicle reference area, m^2 (ft^2)
S_w	wing reference area, m^2 (ft^2)
T_A	wing airload torque, N-m (in-lb)
T_N	wing net torque, N-m (in-lb)
V_A	wing airload shear, N (lb)
V_N	wing net shear, N (lb)
v	true velocity, m/sec (ft/sec)
W	vehicle weight, kg (lb)
W_w	wing weight, kg (lb)
W.S.	wing station
X, Y	longitudinal and lateral axes, respectively

x	longitudinal or chordwise coordinate, m (in.)
$x/\bar{c}$	wing chordwise center of pressure location, percent
y	lateral or spanwise coordinate, m (in.)
y/b	wing spanwise center of pressure location, percent
z	vertical coordinate, m (in.)
α	angle of attack, deg
δ_a	equivalent aileron position, $\frac{\delta_{EL,left} - \delta_{EL,right}}{2}$, deg
δ_{BF}	body flap position, deg
δ_{EL}	elevon position, deg
δ_e	equivalent elevator position, $\frac{\delta_{EL,left} + \delta_{EL,right}}{2}$, deg
δ_r	rudder position, deg
δ_{SB}	speed brake position, deg
ε_i	net output from strain gage i, μm/m (μin/in.)

Subscripts:

i	gage number
α	per degree angle of attack
δ_e	per degree of elevator position
0	zero angle of attack

Subscripts applied to vehicle coordinates:

cg	center of gravity
cp	center of pressure
le	leading edge of wing reference chord

ref	wing reference point
w	wing center of gravity

VEHICLE DESCRIPTION

The orbiter configuration (fig. 1) is a deep boxy fuselage supported on a double delta wing. Elevons are used for pitch and roll control. Split rudders are used for yaw control and also act as speed brakes. A body flap is used for additional pitch trim. Control surface maximum displacements are listed in table 1. The reference geometry used for aerodynamic derivatives are listed in table 2. The mass properties for the ALT configurations are listed in table 3.

The structure is aluminum and is protected against aerodynamic heating by a layer of insulating ceramic tiles. The wing structure (fig. 2) consists of a main box and a glove separated by a wheel well. The main box is composed of 6 spanwise spars with corrugated webs and 12 chordwise ribs with truss webs. The main covers are aluminum skin-stringer aft of the wheel well (F.S. 1191 to 1365) and honeycomb sandwich adjacent to the wheel well (F.S. 1040 to 1191). The glove is composed of truss stub-spars covered with aluminum skin.

PREDICTION TECHNIQUES

Airload predictions were generated by using both theoretical and wind tunnel results. The procedure in the development of the predicted results involved four steps, as follows:

(1) Aerodynamic coefficients and stability derivatives were determined from theoretical calculations or wind tunnel force data.

(2) Surface pressure distribution and resulting shear, bending, and torque loads were determined for given values of angle of attack, Mach number, and surface control position from theoretical calculations or wind tunnel pressure surveys.

(3) Angle of attack and control surface position were determined from a simulator for a given flight condition using results from step (1).

(4) Final airloads were computed for the flight condition using results from steps (2) and (3).

FLEXSTAB Analysis

The FLEXSTAB computer program (ref. 1) provides a potential flow, finite element aeroelastic solution for arbitrary shapes at subsonic and supersonic Mach numbers. The solution produces surface pressures, airframe deflections, and stability derivatives. The stability results have been found to be quite satisfactory for conventional high aspect ratio configurations (ref. 2) but somewhat less satisfactory for low aspect ratio configurations like the YF-12 (ref. 3) and the orbiter (ref. 4) because of the nonpotential flow for these configurations.

The FLEXSTAB orbiter model (fig. 3), which is similar to the model developed in reference 4, consists of 20 control points along the body, 80 panels on the wing, 42 panels on the vertical tail, and 9 panels for the body flap. The model shown was used for subsonic Mach numbers only. Above Mach 1, the body flap was deleted, and for Mach 1.5 and above, the nose was made more conical (surface slope was decreased) to avoid mathematical difficulties. The model was initially run without camber or thickness for the lifting surfaces (that is, as a flat plate). Later camber or thickness was introduced by using the airfoil geometry from references 4 and 5. This produced marked improvement in trim, hinge moment, and wing chordwise center of pressure predictions. Since reference 4 found little aeroelastic effect, only the rigid case was examined. To predict loads, the surface pressures were integrated by using a follow-on computer program to obtain shear, bending, and torque load components at the flight measurement stations. Solutions for several α, δ_e combinations were integrated to obtain wing loads.

Then coefficients were generated to express the loads as functions of α and δ_e. For example,

$$V_A = (C_{V_0} + C_{V_\alpha}\alpha + C_{V_{\delta_e}}\delta_e)\bar{q}$$

$$B_A = (C_{B_0} + C_{B_\alpha}\alpha + C_{B_{\delta_e}}\delta_e)\bar{q}$$

$$T_A = (C_{T_0} + C_{T_\alpha}\alpha + C_{T_{\delta_e}}\delta_e)\bar{q}$$

Elevon hinge moments were also expressed in this fashion. These equations permit the prediction of the loads for any flight condition where $\bar{q}$, α, and δ_e are defined. Body flap, rudder, and speed brake positions were assumed to be zero for the analysis of the selected pitch maneuvers.

Wind Tunnel Data

Models from 0.004 to 0.0405 scale were tested in tunnels at NASA Langley, Ames, and Johnson, at the Arnold Engineering Development Center (AEDC), and at Rockwell (Los Angeles Division) to obtain force and surface pressure data (refs. 6 and 7). The surface pressures were edited, adjusted to agree with force data, and integrated to obtain wing loads for various α, δ_e combinations. Load coefficients were derived from these results in the same form as used for the FLEXSTAB results.

Trim Predictions

To obtain predictions of α and δ_e for the dynamic flight test cases, stability derivatives were entered into a standard six-degree-of-freedom simulation computer program which yielded time histories of α, δ_e, and N_z for a given pilot input time history. The ALT control stick steering control mode (CSS) was represented in the simulation.

FLIGHT TEST TECHNIQUE

Instrumentation

The parameters available from the onboard recording system tape for defining flight condition were Mach number, angle of attack, control surface positions, cockpit acceleration, and rate gyro output. Ground tracking provided altitude, velocity, and dynamic pressure.

Calibrated strain gages were used to measure wing loads. As shown in figure 4, a line of gages was installed along W.S. 134, with axial gages on the upper and lower spar caps, and rosettes on the spar webs and upper and lower skin covers. Elevon actuators were instrumented with pressure transducers to determine hinge moment.

Calibration

In accordance with the procedure presented in reference 8, which was used successfully on the YF-12 airplane (ref. 3), a series of concentrated loads was applied to the instrumented wing at the locations indicated in figure 5. The resulting gage outputs were recorded on a sensitive data acquisition system and used to derive a set of linear equations expressing the wing shear, bending, and torque loads (referenced to W.S. 134 and F.S. 1135) due to air and inertia loads acting outboard of W.S. 134. The derivation followed the least-square multiple linear regression technique described in reference 8.

The load equations take the form:

$$V_N = \sum_i a_{v_i} \varepsilon_i$$

$$B_N = \sum_i a_{b_i} \varepsilon_i$$

$$T_N = \sum_i a_{t_i} \varepsilon_i$$

Flight Data Processing

The data from the onboard recorder were reduced to engineering units at JSC and sent to DFRC on tape. After correction for zero shift, the strains were substituted into the load equations from the calibration to obtain loads. Pitch rate was differentiated to obtain pitching acceleration. Pitching acceleration and cockpit linear acceleration were combined to obtain load factor (N_z) at the center of gravity. Finally, the net loads were corrected for inertia loads to obtain airloads using the following relations:

$$V_A = V_N + (N_z - 1)W_w$$

$$B_A = B_N + (N_z - 1)W_w(y_w - y_{ref})$$

$$T_A = T_N + (N_z - 1)W_w(x_w - x_{ref})$$

where the wing weight and center of gravity are as given in table 4. Elevon hinge moments were computed from measured pressures and elevon geometry. These data, along with condition parameters, were output to printer and plotter.

Flight Maneuvers

The ALT program consisted of a series of flights where the orbiter, mounted on top of a modified B-747 airplane, was carried to an altitude of 6096 to 7620 meters (20,000 to 25,000 feet) and released for unpowered glide flights terminating in landings on Rogers Dry Lake at Edwards, Calif. ALT flights were designated inert captive (IC), captive active (CA), or free flight (FF), depending on the orbiter's status (inert or active) and whether the orbiter was actually released (captive or free). Flights FF1 to FF3 were flown with a tail cone attached to reduce the buffeting of the B-747 empennage and were thus not completely representative of the orbiter flight configuration. However, flights FF4 and FF5 were flown with tail cone off, corresponding to the configuration to be used for actual

orbital flights. FF5 was chosen for this study. Figure 6 shows the time history of altitude, speed, and dynamic pressure for flight FF5 from launch to landing, taken from ground tracking data. The launch was made at an altitude of 5944 meters (19,500 feet) and Mach 0.55 and lasted for 1.8 minutes.

Figures 7(a) and 7(b) show selected parameter time histories for the flight. In figure 7(a), the upper graph plots angle of attack and Mach number, the middle graph plots body flap and speed brake position, and the lower graph plots elevator and aileron position. From the middle plot it is apparent that the body flap moves from -11.7° to 0.6° at launch and that the speed brake was opened about halfway through the flight and closed just prior to touchdown. The effect of the speed brake activity can be seen in the elevator position time history and in the dynamic pressure plots of figure 6. In figure 7(b), the upper and middle graphs show rudder position and side load factor, while the lower plot shows normal load factor and pitching acceleration. The times for longitudinal and lateral inputs were selected from these plots.

Load Maneuvers

For FF5, a pitch maneuver was performed, as noted in figure 7(b), at Mach 0.52 and a dynamic pressure of 11,060 N/m^2 (231 psf). It reached a maximum load factor of 2.47g. Expanded time history plots for the FF5 pitch maneuver are shown in figures 8(a) and 8(b). An interval was chosen for plotting α, δ_e, and wing loads versus N_z from these pitch time histories for comparison with the wind tunnel and theoretical predictions (fig. 8(b)).

RESULTS AND DISCUSSION

Comparisons of predicted and measured results were made for aerodynamic derivatives, angle of attack, elevon position, elevon hinge moment, and wing airload and center of pressure. Predictions were obtained from FLEXSTAB theory (corresponding to the preliminary design mode) and from wind tunnel data.

Derivatives

Comparisons of theoretical and wind tunnel derivatives are shown in figure 9. The angle of attack derivatives (C_{L_α}, C_{M_α}) show the best overall agreement, peaking at Mach 1.2. Derivatives with respect to elevator position ($C_{L_{\delta_e}}$, $C_{M_{\delta_e}}$) were overpredicted near Mach 1 but were

relatively close elsewhere. Aerodynamic coefficients (C_{L_0}, C_{M_0}) showed the poorest correlation, with predicted C_{L_0} values biased positively and C_{M_0} predictions exhibiting a discontinuity near Mach 1. The lack of correlation in the transonic range is not surprising, considering the linear potential flow aerodynamics in FLEXSTAB.

Trim

Angle of attack and elevator position were obtained from simulator computer runs by using wind tunnel derivatives, theoretically predicted derivatives, and the recorded pilot pitch control input. Time histories for the FF5 pitch maneuvers are shown in figure 10. Flight measured values are compared with wind tunnel and theoretical predictions. The wind tunnel values closely follow the flight measurements, while the theoretical values underpredict load factor and elevator position.

Angle of attack and elevator position are plotted against load factor in figure 11. The figure shows that the slopes of α/g and δ_e/g are predicted quite well by both wind tunnel and the theoretical methods.

Elevon Hinge Moment

Wind tunnel and theoretically derived values are plotted with flight measurements in figure 12. The wind tunnel predictions compare closely with the flight measurements for the inboard surface and are somewhat low for the outboard surface. The theoretical predictions are in close agreement with the flight measurements for both surfaces.

Wing Load and Center of Pressure

Shear (V_A), bending (B_A), and torque (T_A) loads were computed as described above. These values were used to compute the spanwise (y/b) and chordwise ($x/\bar{c}$) locations of the airload center of pressure as shown in figure 13. The variation of these wing load parameters with load factor are shown in figure 14. The three sets of data are for flight, wind tunnel, and theoretical results.

The load varies linearly with load factor. The spanwise center of pressure location is relatively constant, while the chordwise center of pressure is a strong function of elevator position, moving ahead of the leading edge ($x/\bar{c} < 0$) for negative (trailing edge up) elevator positions.

Wind tunnel predictions give a load/g slope close to the flight measured value but overpredict the value by a nearly constant increment.

Wind tunnel predictions of spanwise center of pressure are somewhat outboard but agree closely on chordwise location.

FLEXSTAB predictions are in good agreement for load/g slope. Theoretical predictions of center of pressure location are somewhat inboard spanwise but close chordwise.

CONCLUDING REMARKS

The results of this study led to the following observations regarding the current capability for airload measurement and prediction on a low aspect ratio double delta aerodynamic configuration. First, strain gage load measurement was successful for a low aspect ratio wing. Second, simulation using both wind tunnel and theoretical derivatives produced useful predictions of load factor, angle of attack, and elevator position. And third, FLEXSTAB surface pressure predictions yielded useful predictions for both wing loads and elevon hinge moments.

Dryden Flight Research Center
National Aeronautics and Space Administration
Edwards, California, April 1981

REFERENCES

1. Tinoco, E. N.; and Mercer, J. E.: FLEXSTAB--A Summary of the Functions and Capabilities of the NASA Flexible Airplane Analysis Computer System. NASA CR-2564, 1974.

2. Dornfeld, G. M.; Bhatia, K. G.; Maier, R. E.; Snow, R. N.; and Van Rossum, D. A.: A Method for Predicting the Stability Characteristics of an Elastic Airplane--Volume IV: FLEXSTAB 1.02.00 Demonstration Cases and Results. NASA CR-114715, 1974.

3. NASA YF-12 Flight Loads Program. NASA TM X-3061, 1974.

4. Chyu, Wei J.; Cavin, Ralph K.; and Erickson, Larry L.: Static and Dynamic Stability Analysis of the Space Shuttle Vehicle-Orbiter. NASA TP-1179, 1978.

5. Preisser, John S.; and Lowder, Harold E., Jr.: Comparison of Theoretical and Experimental Steady Wing Loads on a Space Shuttle Configuration at Mach Numbers of 0.6 and 1.4. NASA TM X-3404, 1976.

6. Aerodynamic Design Data Book. Volume I - Orbiter Vehicle. NASA CR-160386, 1978.

7. Airloads Design Data Book. SD72-SH-0060-3H, Rockwell International, March 2, 1979.

8. Skopinski, T. H.; Aiken, William S., Jr.; and Huston, Wilber B.: Calibration of Strain-Gage Installations in Aircraft Structures for Measurement of Flight Loads. NACA Rept. 1178, 1954.

TABLE 1. - CONTROL SURFACE LIMITS

Elevon deflection, positive trailing edge down, deg	-35 to 20
Rudder deflection, positive trailing edge left, deg	±22.8
Speed brake deflection, positive trailing edge open, deg	0 to 87.2
Body flap deflection, positive trailing edge down, deg	-11.7 to 22.55

TABLE 2. - REFERENCE GEOMETRY

S, m^2 (ft^2)	249.91 (2690)
b, m (in.)	23.79 (936.68)
$\bar{c}$, m (in.)	12.06 (474.81)

TABLE 3. - ORBITER 101 FF5 MASS PROPERTIES

W, kg (lb)	68,422.6 (150,846)
x_{cg}, m (in.)	27.76 (1092.8)
z_{cg}, m (in.)	9.45 (372.0)
I_{XX}, kg-m^2 (slug-ft^2)	1.007×10^6 (0.743×10^6)
I_{YY}, kg-m^2 (slug-ft^2)	7.510×10^6 (5.539×10^6)
I_{ZZ}, kg-m^2 (slug-ft^2)	7.827×10^6 (5.773×10^6)
I_{XZ}, kg-m^2 (slug-ft^2)	0.175×10^6 (0.129×10^6)

TABLE 4. - ORBITER WING REFERENCE PROPERTIES

W_w, kg (lb)	5825.94 (12,844)
y_w, m (in.)	6.0 (236.2)
x_w, m (in.)	31.74 (1249.8)
$\bar{c}_w$, m (in.)	9.21 (365)
b_w, m (in.)	8.48 (334)
x_{le}, m (in.)	28.32 (1115)
x_{ref}, m (in.)	28.83 (1135)
y_{ref}, m (in.)	2.67 (105)

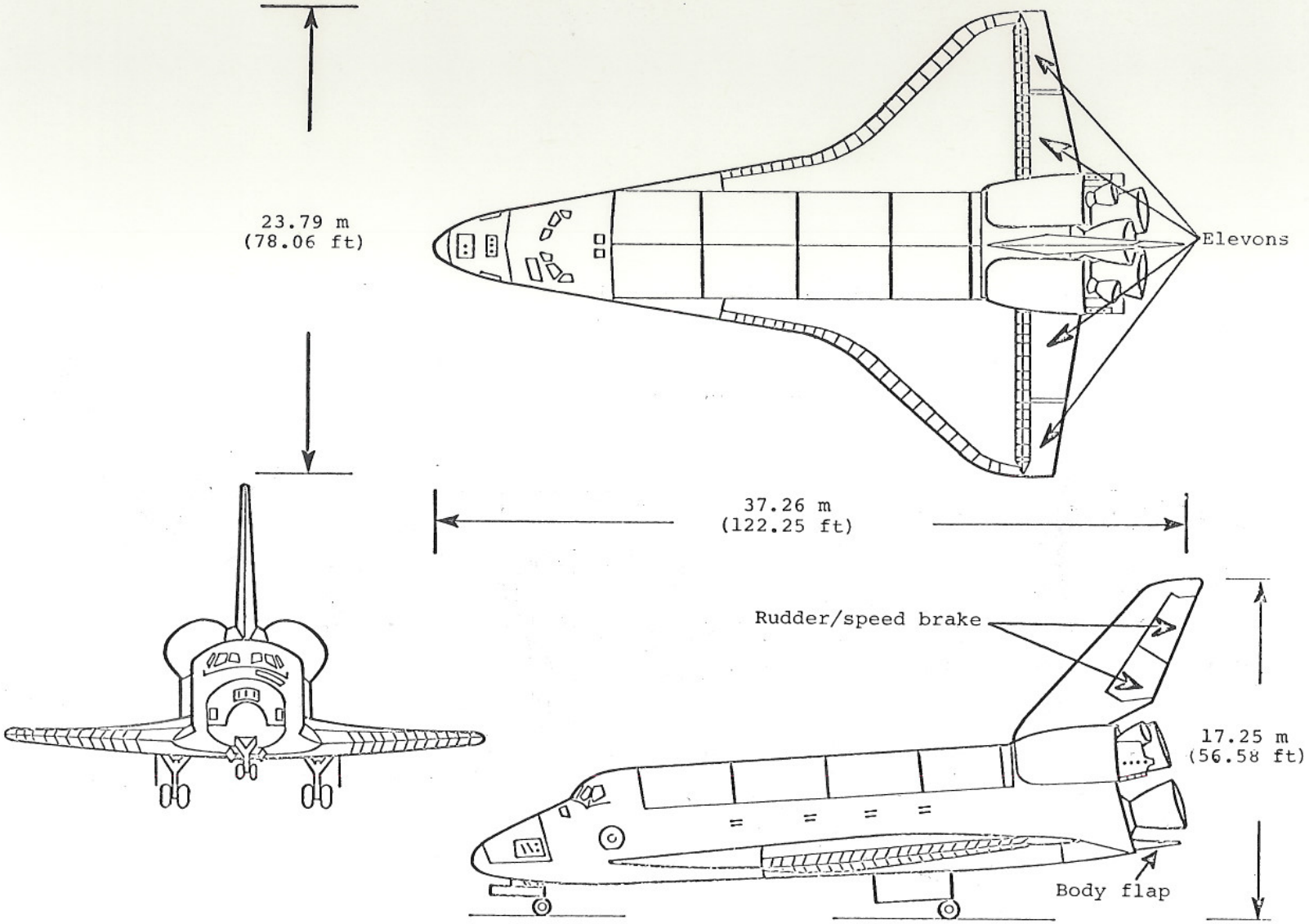

Figure 1. Orbiter configuration.

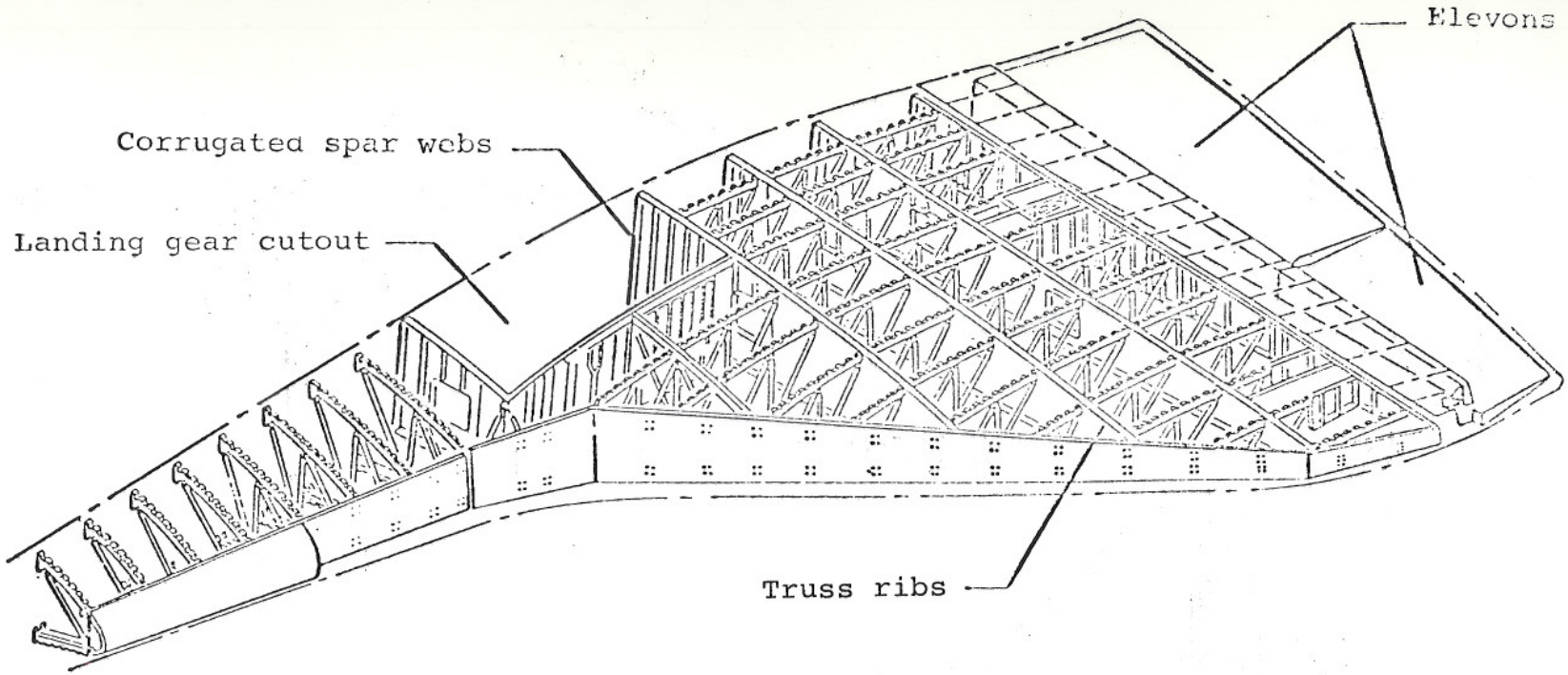

Figure 2. Orbiter internal wing structure.

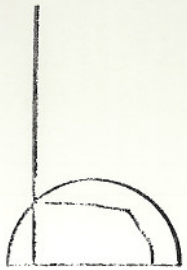

Front view

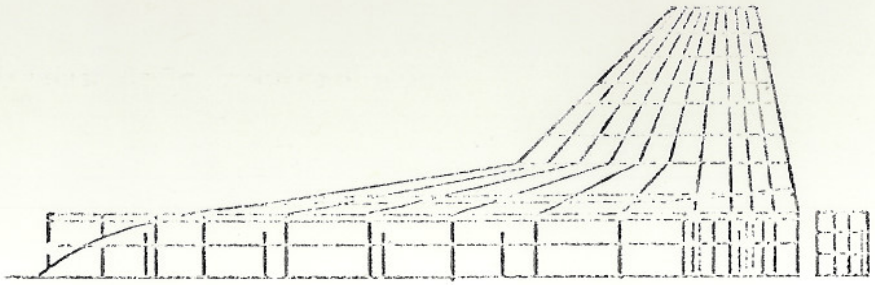

Top view

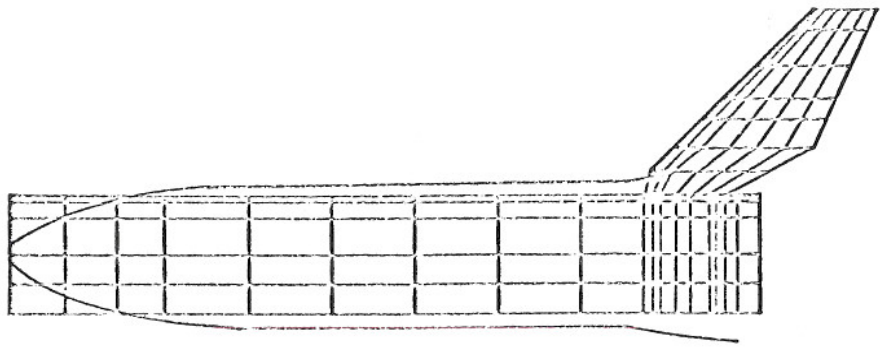

Side view

Figure 3. FLEXSTAB aerodynamic model. (Computer plot does not show actual body camber.)

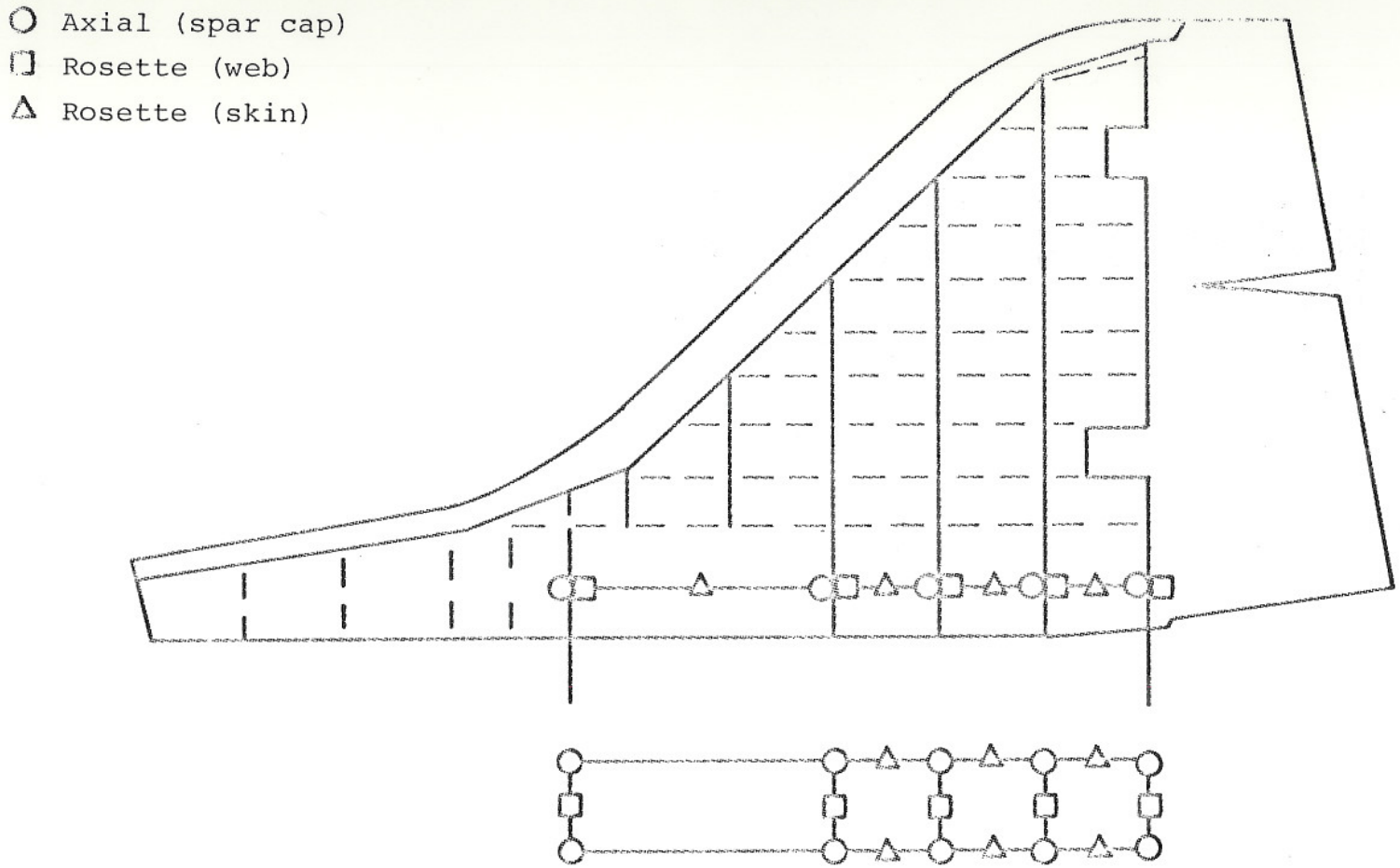

Figure 4. Strain gage locations.

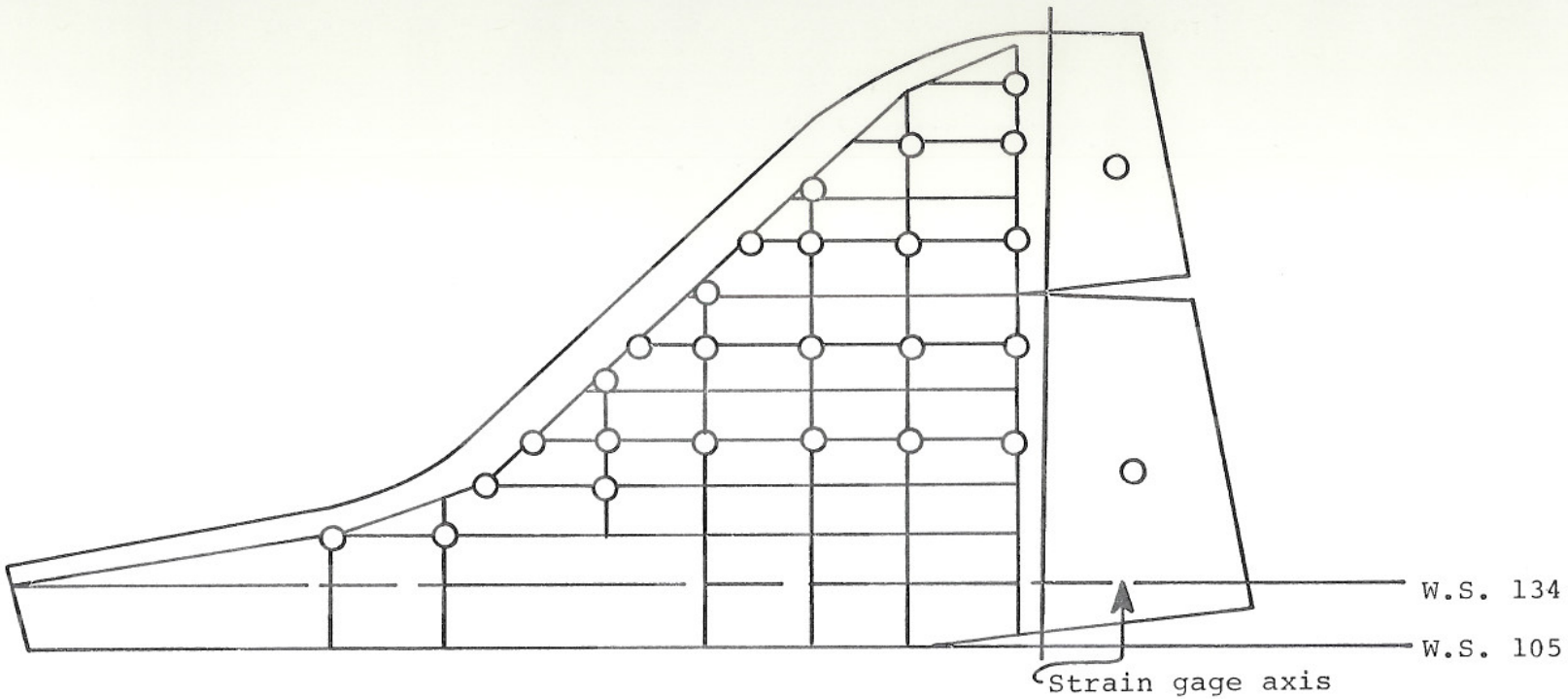

Figure 5. Calibration condition load locations.

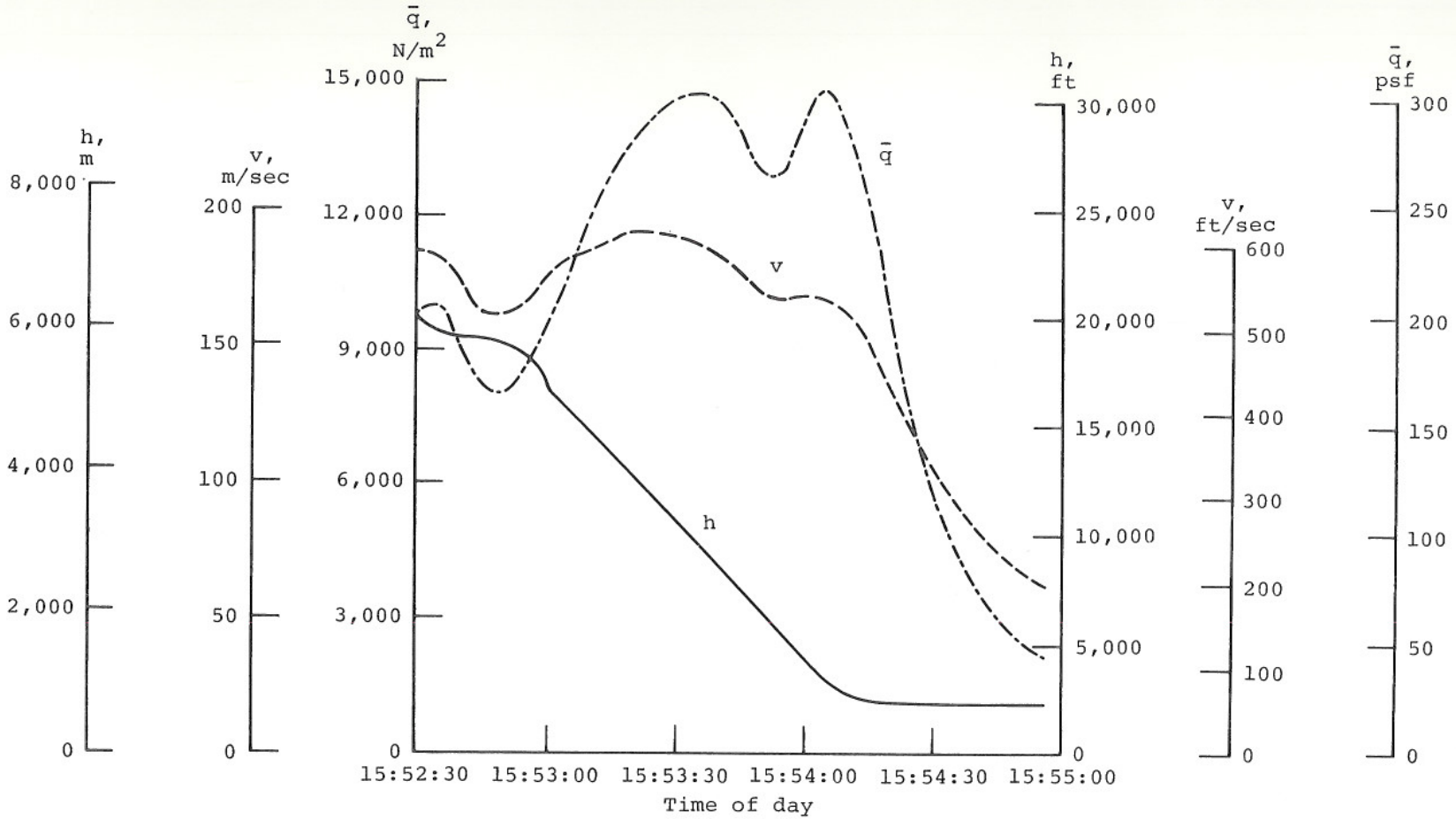

Figure 6. Altitude/speed/dynamic pressure time history for FF5.

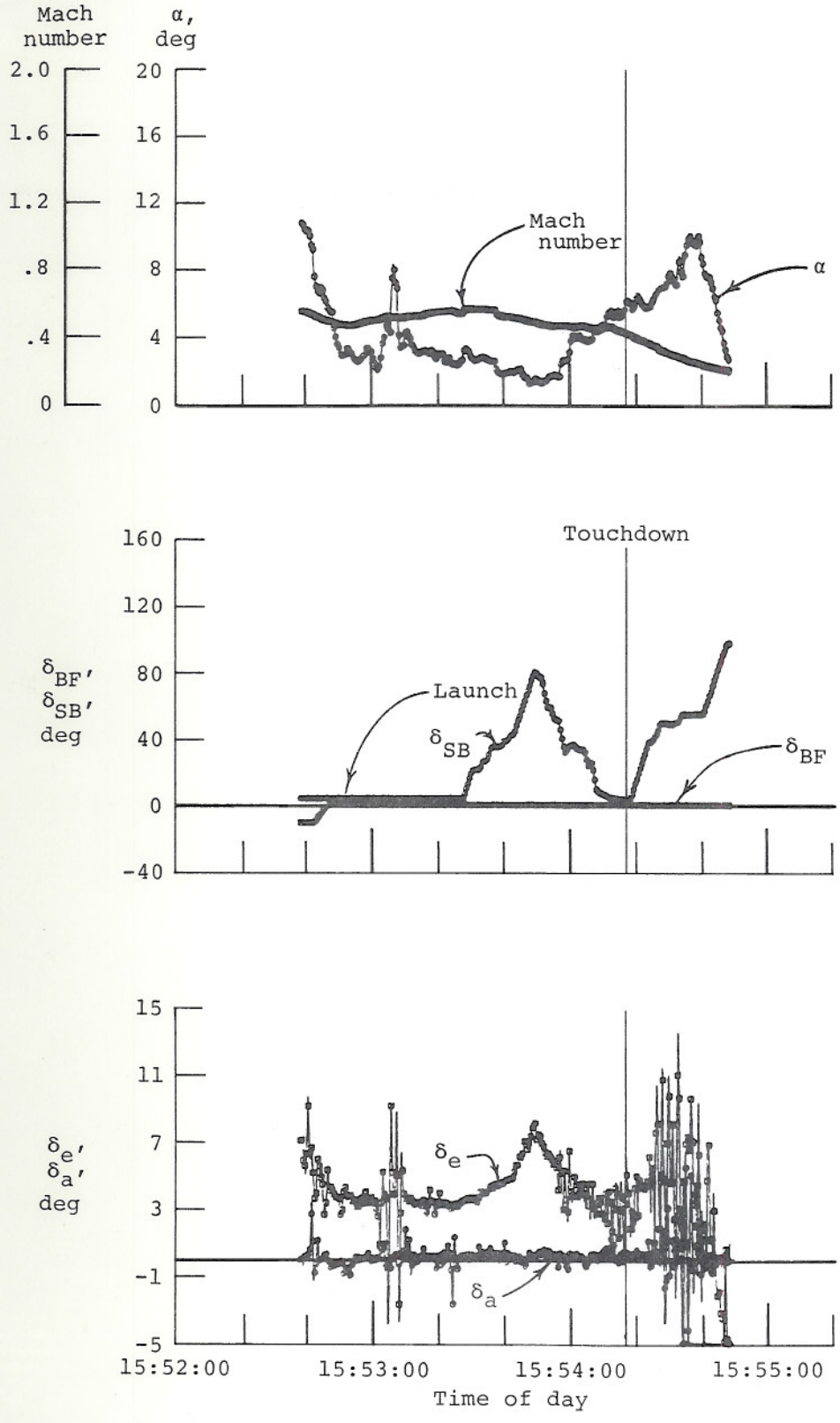

Figure 7. FF5 flight time history.

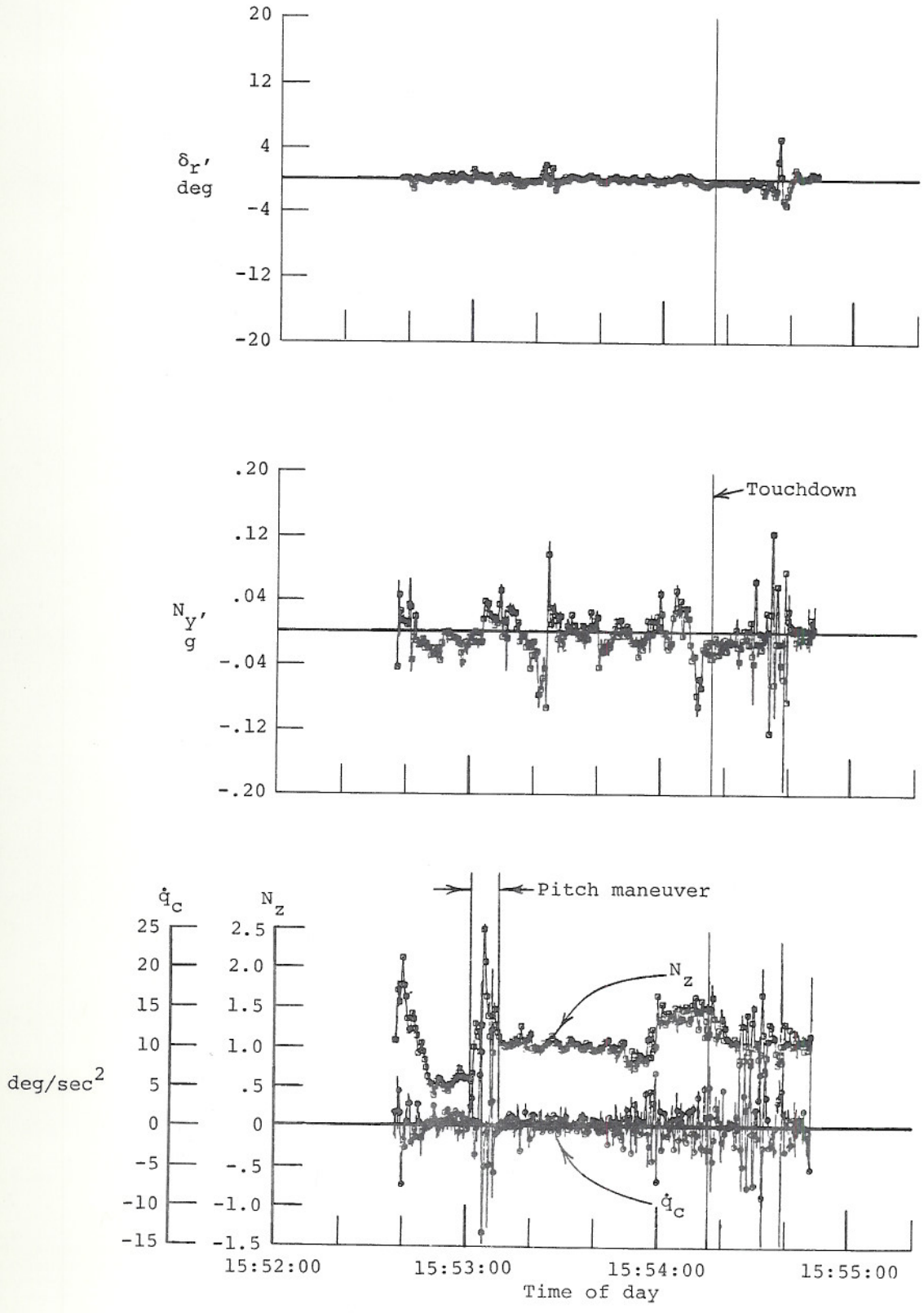

Figure 7. Concluded.

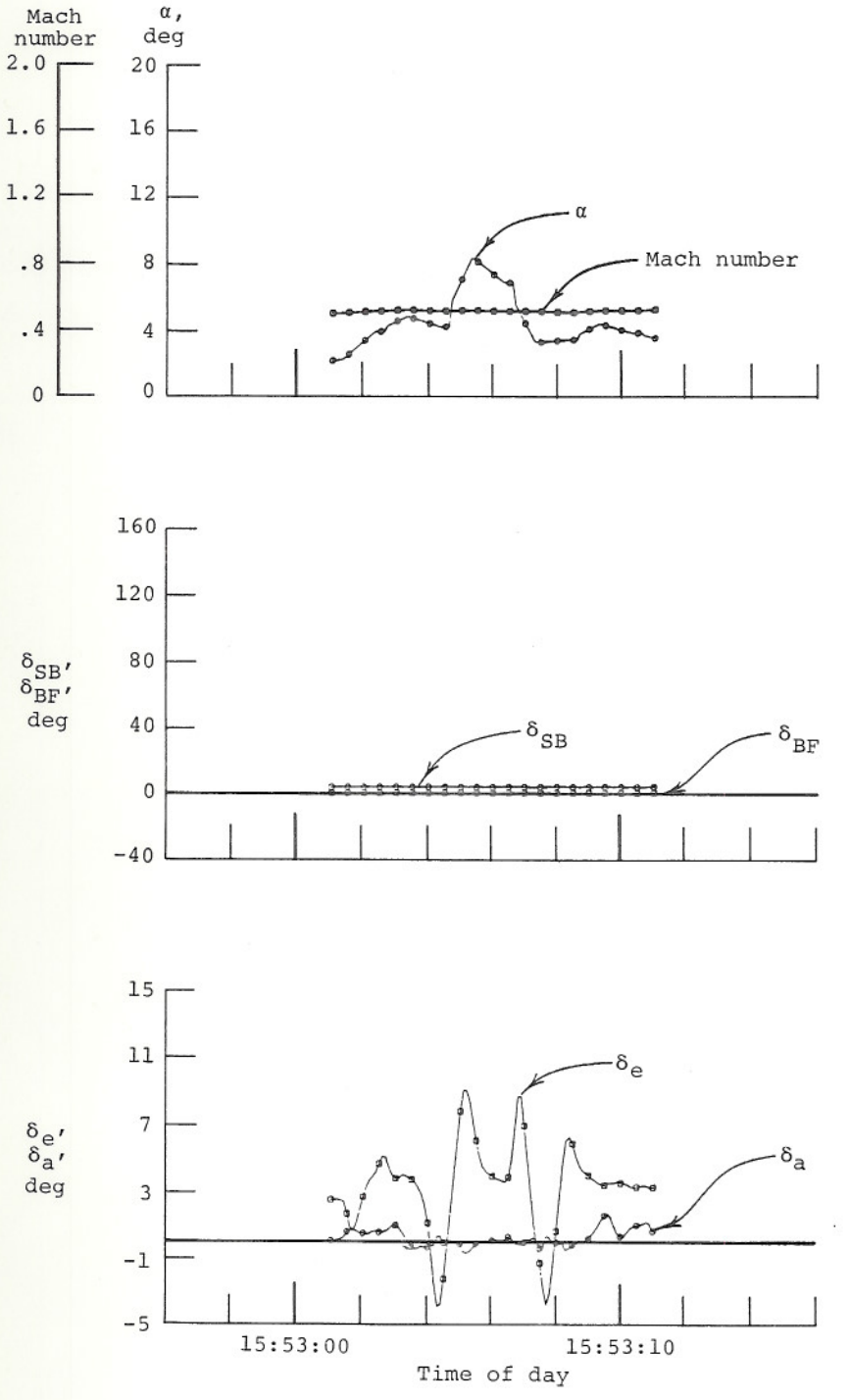

Figure 8. FF5 pitch maneuver time history.

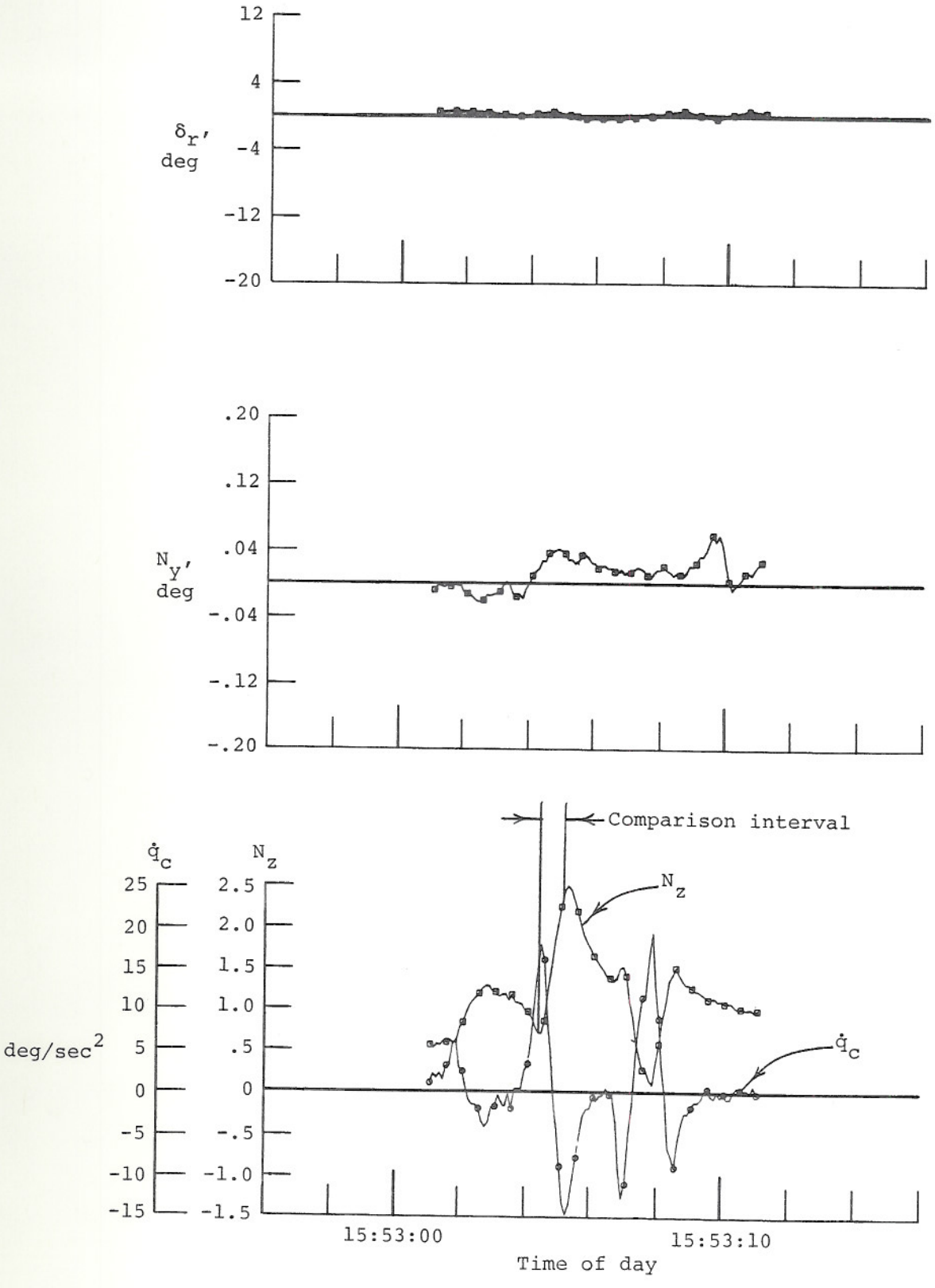

Figure 8. Concluded.

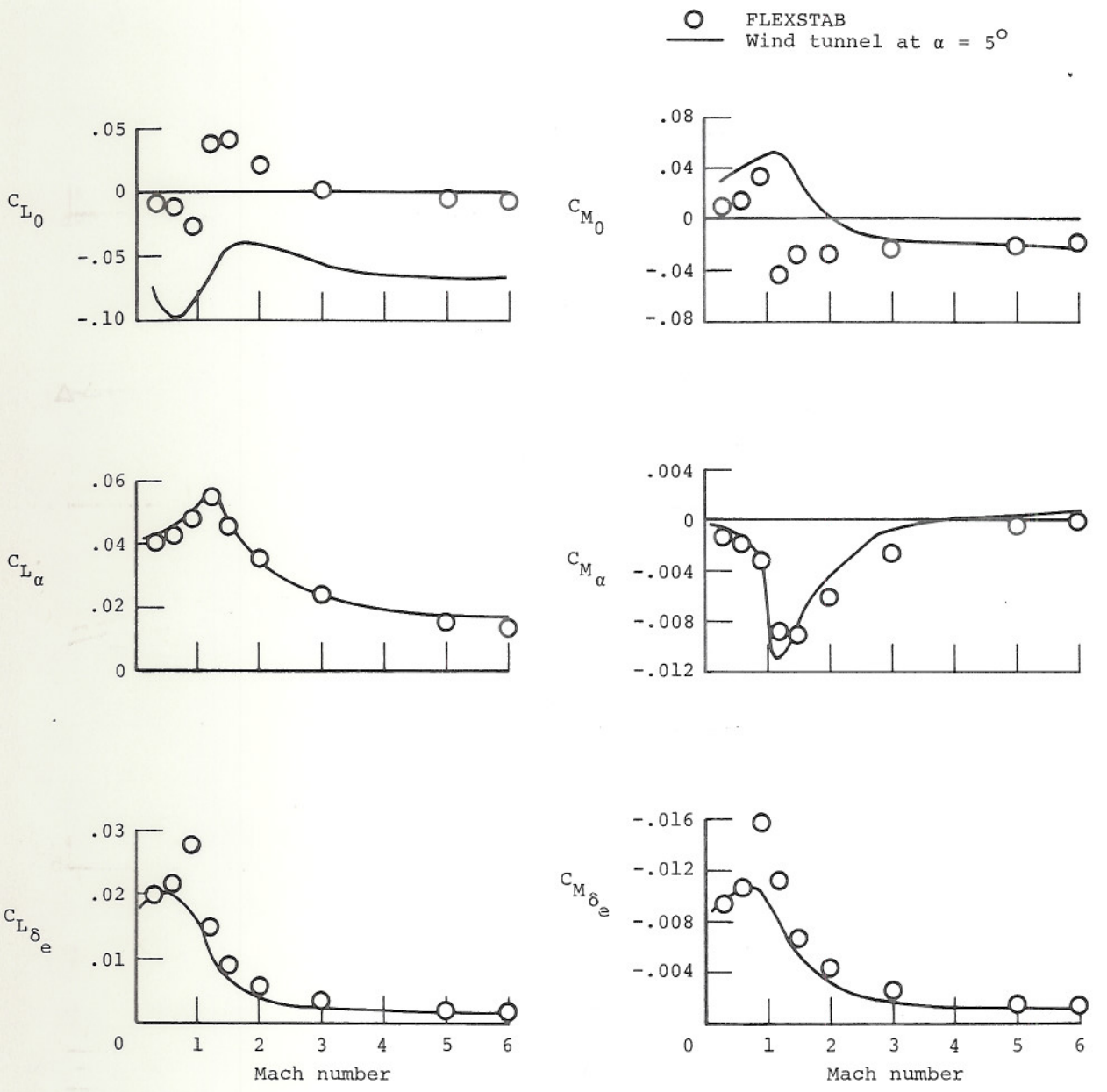

Figure 9. Orbiter aerodynamic derivatives versus Mach number. Center of gravity = 0.65 L_B (F.S. 1076.7).

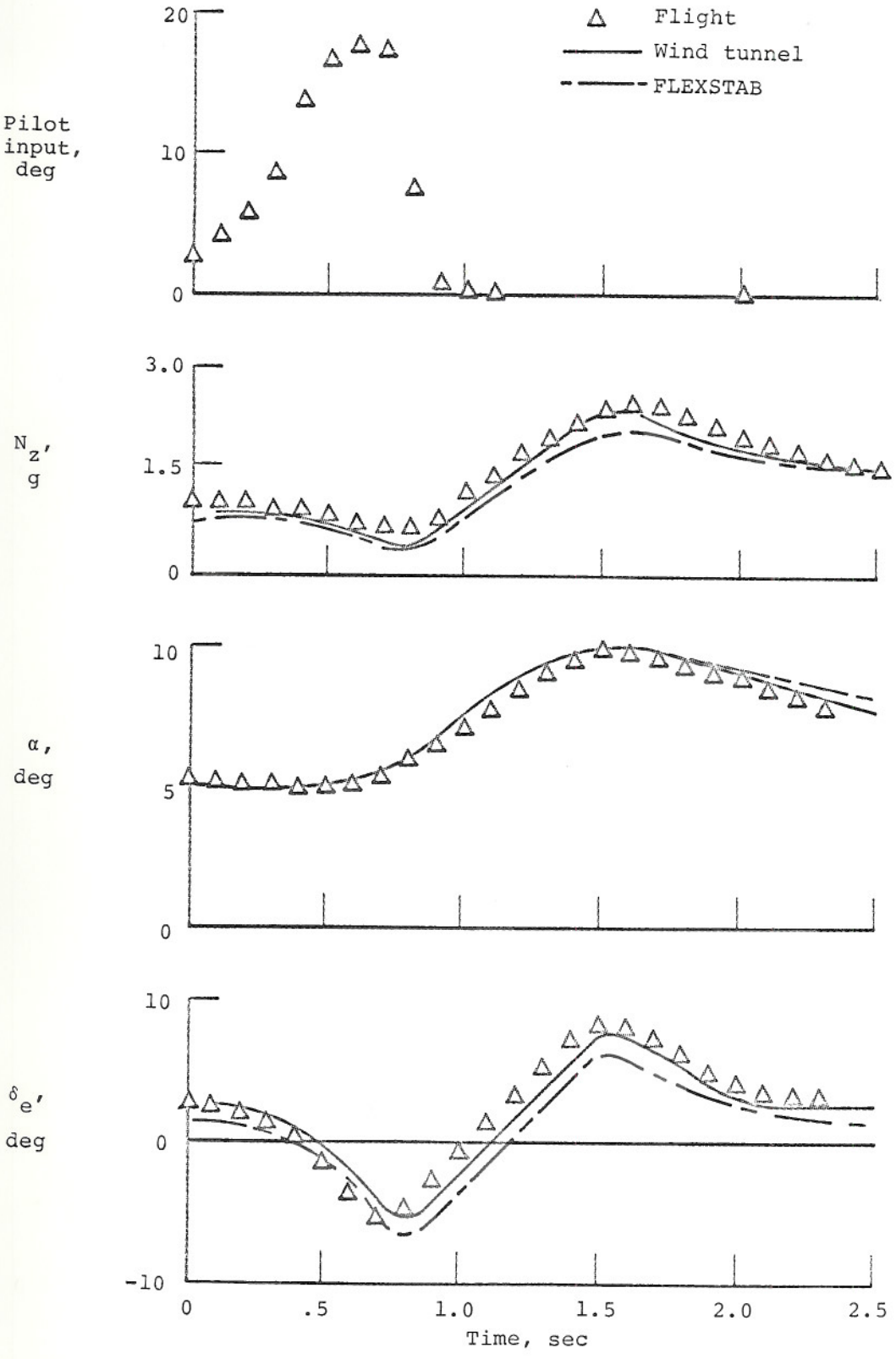

Figure 10. Maneuver time history. Flight versus simulation.

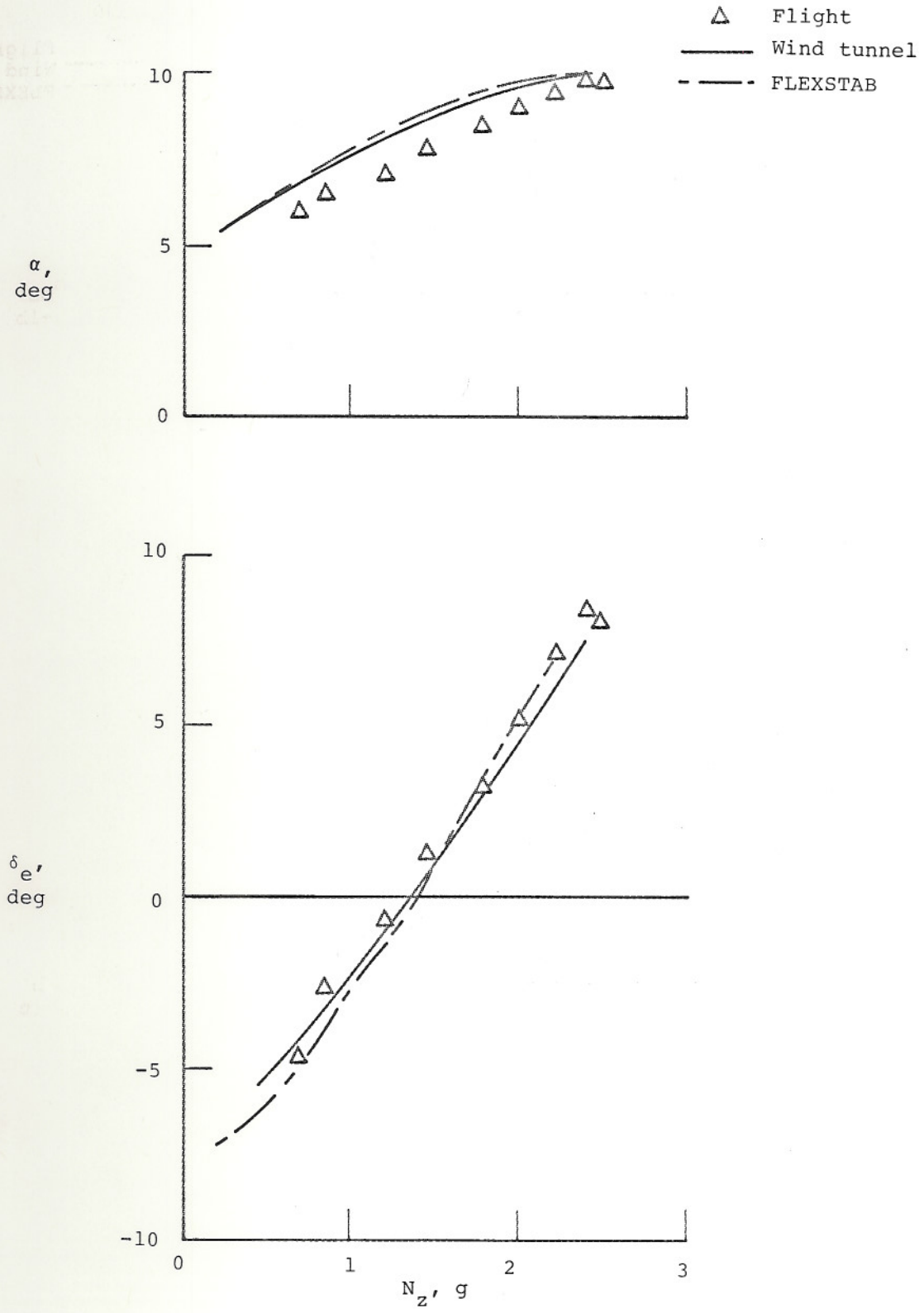

Figure 11. Angle of attack and elevon position versus load factor.

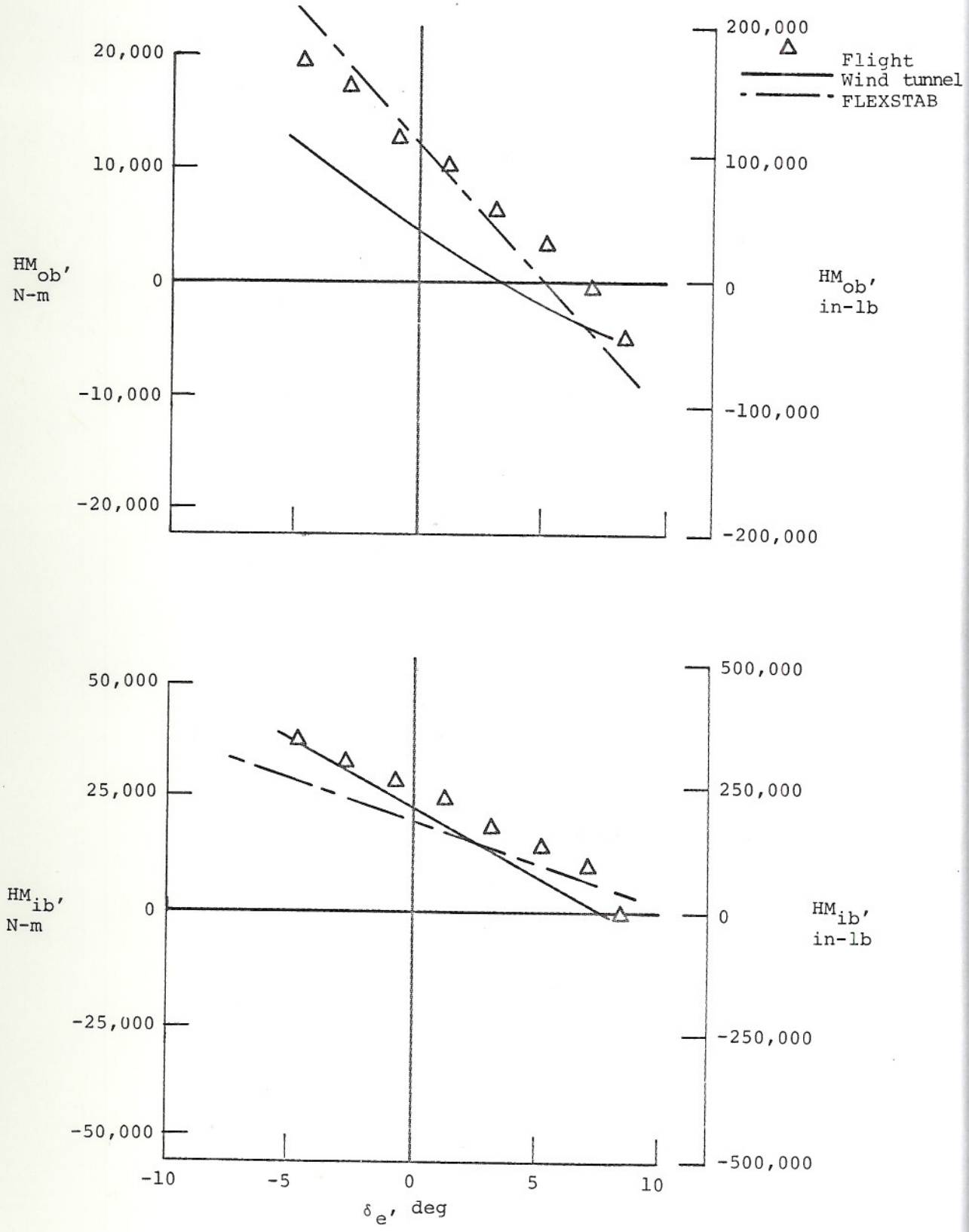

Figure 12. Hinge moment versus elevon deflection.

$$x_{cp} = x_{ref} - (T_A/V_A)$$
$$y_{cp} = y_{ref} + (B_A/V_A)$$
$$x/\bar{c} = (x_{cp} - x_{le})/\bar{c}_w$$
$$y/b = (y_{cp} - 134)/b_w$$

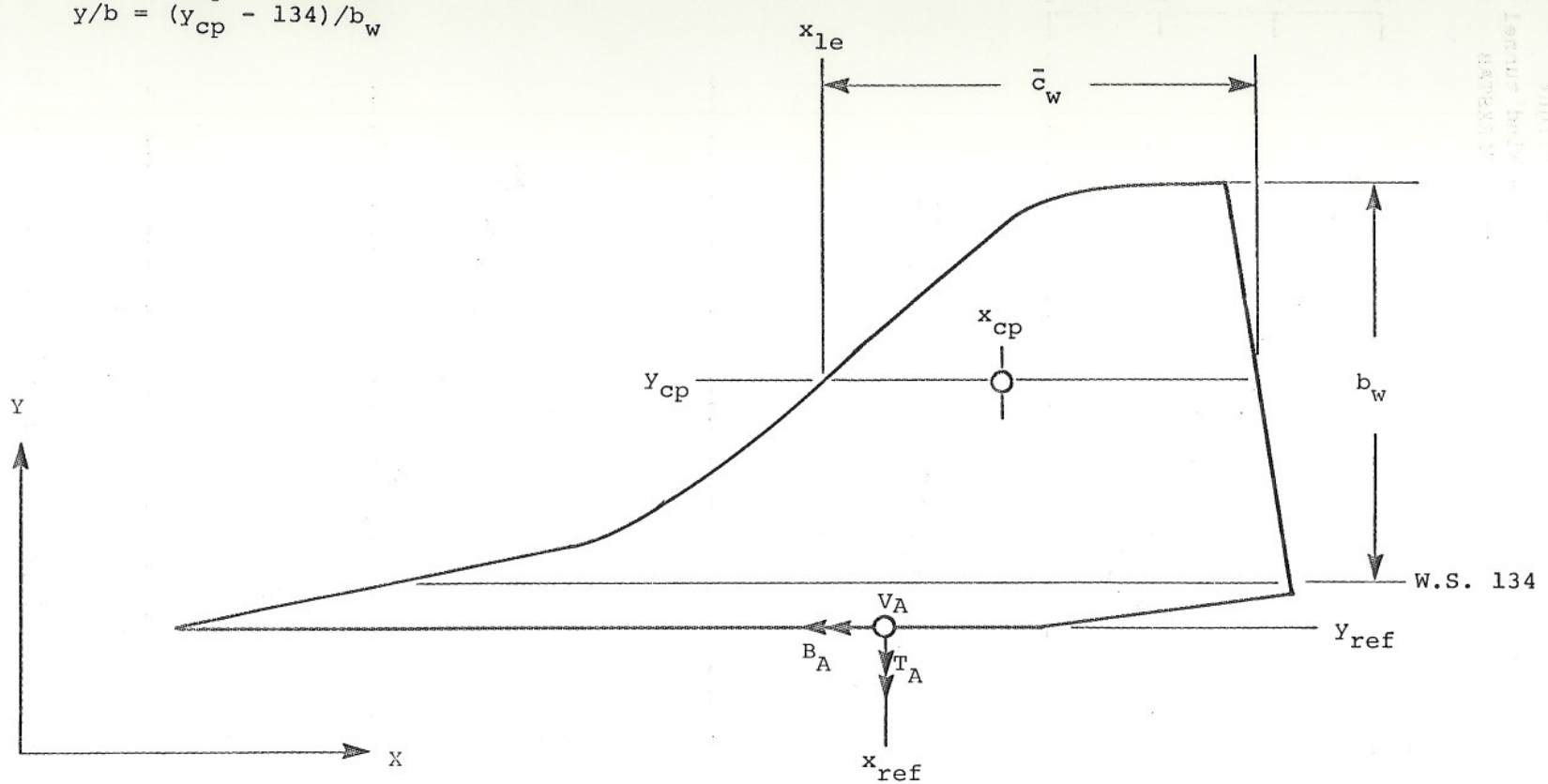

Figure 13. Wing center of pressure geometry.

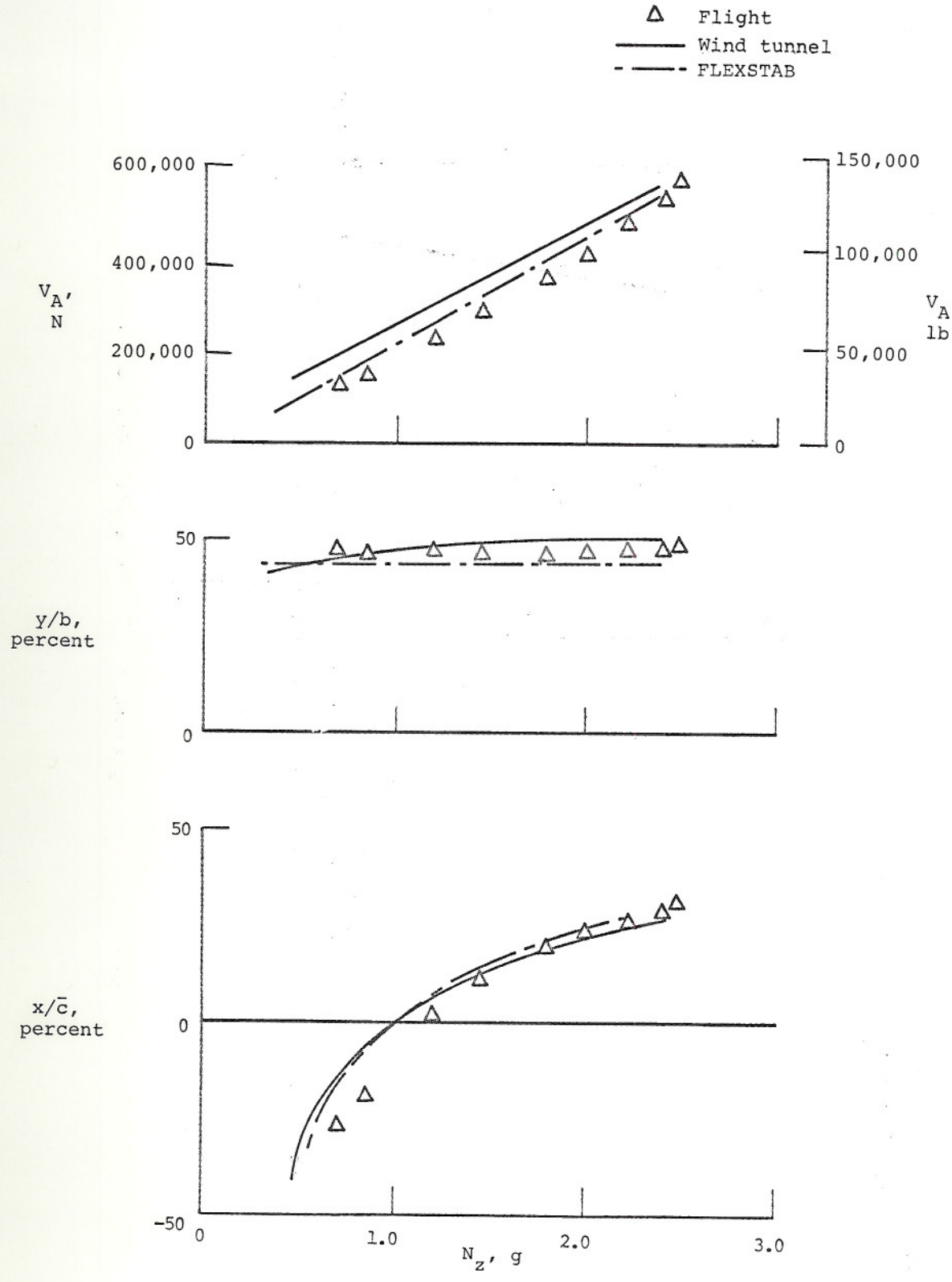

Figure 14. Wing load and center of pressure versus load factor.

1. Report No.	2. Government Accession No.	3. Recipient's Catalog No.
NASA TM-81358		

4. Title and Subtitle	5. Report Date
COMPARISON OF THEORETICAL PREDICTIONS OF ORBITER AIRLOADS WITH WIND TUNNEL AND FLIGHT TEST RESULTS FOR A MACH NUMBER OF 0.52	May 1981
	6. Performing Organization Code 989-10-00

7. Author(s)	8. Performing Organization Report No.
Alan L. Carter and Robert L. Sims	

9. Performing Organization Name and Address	10. Work Unit No.
Dryden Flight Research Center P.O. Box 273 Edwards, California 93523	11. Contract or Grant No.

12. Sponsoring Agency Name and Address	13. Type of Report and Period Covered
National Aeronautics and Space Administration Washington, D.C. 20546	Technical Memorandum
	14. Sponsoring Agency Code

15. Supplementary Notes

16. Abstract

This paper discusses the measurement and prediction of wing airloads for space shuttle orbiter 101 during approach and landing tests. Strain gage instrumentation, calibration, and flight data processing are discussed, along with wind tunnel and simulator results. The generation of theoretical predictions using the FLEXSTAB computer program is described, and the results are compared to experimental measurements.

17. Key Words (Suggested by Author(s))	18. Distribution Statement
Space shuttle orbiter Airload prediction Airload measurement FLEXSTAB	Unclassified - Unlimited STAR category 05

19. Security Classif. (of this report)	20. Security Classif. (of this page)	21. No. of Pages	22. Price*
Unclassified	Unclassified	33	A03

*For sale by the National Technical Information Service, Springfield, VA 22161